



# Pressure-temperature phase diagram of LiBH<sub>4</sub>: Synchrotron x-ray diffraction experiments and theoretical analysis

V. Dmitriev,\* Y. Filinchuk, and D. Chernyshov

Swiss-Norwegian Beam Lines at ESRF, Boite Postale 220, F-38043 Grenoble, France

A. V. Talyzin, A. Dzwilewski, O. Andersson, and B. Sundqvist

Department of Physics, Umeå University, SE-90187 Umeå, Sweden

A. Kurnosov

Bayerisches Geoinstitut, Universität Bayreuth, D-95440 Bayreuth, Germany

(Received 3 April 2008; revised manuscript received 21 April 2008; published 16 May 2008; corrected 8 September 2008)

An *in situ* combined high-temperature high-pressure synchrotron radiation diffraction study has been carried out on LiBH<sub>4</sub>. The phase diagram of LiBH<sub>4</sub> is mapped to 10 GPa and 500 K, and four phases are identified. The corresponding structural distortions are analyzed in terms of symmetry-breaking atomic position shifts and anion ordering. Group-theoretical and crystal-chemical considerations reveal a nontrivial layered structure of LiBH<sub>4</sub>. The layers and their deformations define the structural stability of the observed phases.

DOI: [10.1103/PhysRevB.77.174112](https://doi.org/10.1103/PhysRevB.77.174112)

PACS number(s): 61.05.cp, 61.50.Ks, 61.66.Fn

## I. INTRODUCTION

Light metal borohydrides are promising materials for hydrogen storage applications. While it was recently shown that the lightest borohydride, LiBH<sub>4</sub>, desorbs hydrogen reversibly,<sup>1</sup> its stability with respect to thermal decompositions remains the major drawback for practical use. One way to approach the problem is to chemically destabilize borohydrides. Indeed, the high reactivity of LiBH<sub>4</sub> (Ref. 2) allows destabilization via chemical reaction with other hydrogen-rich substances, such as LiNH<sub>2</sub> and MgH<sub>2</sub>.<sup>3,4</sup> Thus, a practically useful hydrogen storage system might be found among the numerous possible combinations. It was argued<sup>5</sup> that the high-temperature and high-pressure phases of light borohydrides might serve as targets for obtaining improved material by chemical substitutions.

Another widely used approach is *ab initio* modeling of crystal structures and physical-chemical transformations as a function of external stimuli. However, in the case of light borohydrides, this approach seems to have a very limited predictive power; the temperature and pressure evolution of the sodium and lithium borohydride structures may serve as an illustration. NaBH<sub>4</sub>, a borohydride that shows a remarkable chemical and thermal stability, was among the first systems studied experimentally in a wide range of temperatures and pressures, as well as theoretically. At ambient conditions, NaBH<sub>4</sub> has a cubic structure that, despite its simplicity, has been described earlier in the different space groups *Fm-3m* (Ref. 6) and *F-43m*,<sup>7,8</sup> while a recent revision confirms the centrosymmetric *Fm-3m*.<sup>9</sup> A closely related tetragonal structure, with either *P-42<sub>1</sub>c* or *P4<sub>2</sub>/nmc* symmetry, appears on cooling to  $\sim 180$  K or upon compression to  $\sim 2$  GPa.<sup>10</sup> Above  $\sim 9$  GPa, yet another phase was detected by diffraction and Raman spectroscopies, but both experiment and theory originally failed to identify its structure.<sup>11,12</sup> Only recently, it was shown to be of the BaSO<sub>4</sub> type.<sup>13</sup> Such difficulties in identifying and predicting even the relatively simple NaBH<sub>4</sub> phases impede rational attempts to influence the stability of borohydrides.

Significant efforts have been recently made to understand the structural properties of LiBH<sub>4</sub>. At ambient conditions, it has an orthorhombic *Pnma* structure,<sup>14,15</sup> which is different from the structures of all other alkali metal borohydrides. No phase transition has been found in LiBH<sub>4</sub> at low temperature, but a transformation occurs on heating to 381 K.<sup>14-19</sup> The structure of the high-temperature phase (denoted here as phase I) has been studied recently in detail, both experimentally and theoretically. According to the most recent experimental data (neutron powder diffraction<sup>15</sup> and synchrotron diffraction on single crystals<sup>20</sup>), the structure of this phase is *P6<sub>3</sub>mc*, but theoretical studies find the phase with this symmetry unstable and suggest *Cc* (Ref. 21) and *P3* structures.<sup>22</sup>

The pressure evolution of LiBH<sub>4</sub> is even more complicated. A careful volumetric study of the pressure-temperature (*P-T*) phase diagram of LiBH<sub>4</sub> was carried out by Pistorius<sup>23</sup> about 40 years ago and until recently, it remained the only available experimental study in this field. Pistorius identified five different *P-T* regions at pressures below 4.5 GPa and temperatures below 600 K, but the structures of the high-pressure phases remained unknown until recently (see Fig. 1). At ambient temperature, a phase transition from the *Pnma* phase (denoted II here) into the almost 6% denser high-pressure phase (denoted III here) was observed at around 0.6 GPa at 298 K and 0.84 GPa at 341 K.<sup>23</sup> The phase transition was recently confirmed by Raman spectroscopy, thermal conductivity measurements, differential thermal analysis (DTA), and x-ray diffraction (XRD) and could be accurately mapped down to 100 K.<sup>24</sup> Various structures were theoretically predicted for this high-pressure phase of LiBH<sub>4</sub>: the cubic NaBH<sub>4</sub>-type structure above 6.2 GPa (Ref. 25) and monoclinic *P2<sub>1</sub>/c* and *Cc* structures, respectively, at  $\sim 1$  GPa (Ref. 26) and  $\sim 2.2$  GPa,<sup>21</sup> but none of them were consistent with diffraction data.<sup>24</sup>

Very recently, a detailed diffraction study of phase transitions in LiBH<sub>4</sub> at room temperature and pressures up to 18 GPa was performed by using synchrotron radiation.<sup>5</sup> It was shown that phase III has a pseudotetragonal structure

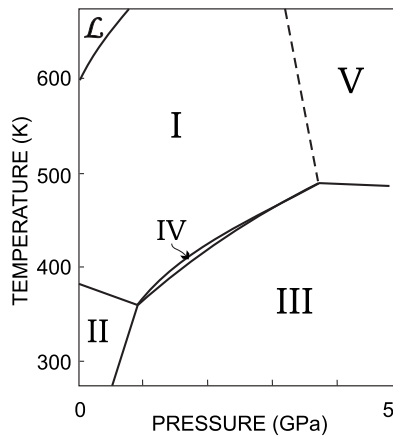


FIG. 1. Partial  $P$ - $T$  phase diagram of  $\text{LiBH}_4$  according to Ref. 23.

with  $Ama2$  symmetry. It also revealed that phase III crystallizes in a structure type, where the  $\text{BH}_4$  anion has an unprecedented square-planar coordination by four Li atoms. Considering the fact that this arrangement was entirely unexpected, it comes as no surprise that the theoretical attempts to predict it were doomed to failure. A second transformation was found at higher pressures. This started at 8 GPa and was not yet completed at 18 GPa, the maximum pressure achieved in these experiments. The structure of the new phase (originally denoted VI) was found<sup>5</sup> to be of the cubic  $\text{NaBH}_4$  type, space group  $Fm\bar{3}m$ . It is interesting that the cubic structure was predicted for  $\text{LiBH}_4$  at high pressure from simple geometrical considerations.<sup>23</sup>

Summarizing the previously published experimental works, we found that six phase regions were identified in the experimental  $P$ - $T$  diagram of  $\text{LiBH}_4$ , but the corresponding crystal structures are found only for four of them.  $P$ - $T$  regions IV and V have been observed only in the early study by Pistorius<sup>23</sup> by detecting the phase boundaries by DTA, and thus no structural information is available for them.

The apparent complexity of the pressure and temperature response of seemingly simple light borohydrides, the disagreement between theoretical calculations and experiment, and the limited amount of structural data, all call for more experimental and theoretical efforts. A step toward a unified picture of the phase transformations could be a set of diffraction experiments evaluating symmetry changes and structural deformations, followed by a group-theoretical analysis in the framework of Landau theory. Self-consistency of the symmetry analysis also serves as a validation of the crystal structures uncovered in diffraction experiments. As far as we are aware, such a study, which should normally precede detailed microscopic modeling, has not been done yet.

Here, we present results of high-pressure-high-temperature synchrotron diffraction experiments on  $\text{LiBH}_4$  in diamond anvil cells (DACs) of up to 10 GPa and 500 K. We extended the mapping of the  $\text{LiBH}_4$  phase diagram and identified the nature of the  $P$ - $T$  regions IV and V, both by diffraction and by thermal conductivity and DTA measurements. We also present here a phenomenological analysis of the phase transitions observed in this system.

## II. EXPERIMENTAL DETAILS

$\text{LiBH}_4$  of 99.9% purity was purchased from Sigma-Aldrich and used without additional purification. Raman spectra and XRD data recorded on the powder samples at ambient conditions indicated the presence of a single  $\text{LiBH}_4$  phase and showed no diffraction peaks from impurities. High-pressure experiments were performed using a resistively heated DAC with 0.4–0.6 mm flat culets. The sample was loaded into a 0.2–0.4 mm hole in the rhenium or iron gasket together with a ruby chip and in some cases with a piece of gold wire, both used for pressure calibration. No pressure medium was used. The initial thickness of the sample was 60–70  $\mu\text{m}$ . Since the material is sensitive to moisture, the loading was performed in a glovebox under argon gas. Raman spectra of the starting material and of the sample loaded into the DAC were identical, which confirmed that the loading procedure had not affected the sample.

*In situ* high-pressure XRD data were measured at the Swiss-Norwegian Beam Line (BM1A) ( $\lambda=0.711360$  Å) and the ID09a beamline ( $\lambda=0.41125$  Å) of the European Synchrotron Radiation Facility (ESRF, Grenoble, France). Two-dimensional diffraction images were analyzed using the ESRF FIT2D software, yielding one-dimensional intensity vs diffraction angle patterns. Diffraction measurements were performed in five separate experiments, each of them in various pressure-temperature intervals. Maximum pressures up to 20.6 GPa (at ambient temperature) and temperatures up to 500 K (at 1–8 GPa) were used. The data were processed using FULLPROF suite<sup>27</sup> to yield cell parameters and structural information.

The thermal conductivity was measured for the low-pressure phases up to 1.2 GPa in a separate experiment, using the same hot wire method as in the earlier study<sup>24</sup> and with the same piston-cylinder high-pressure equipment. Again, two thermocouples were placed in the cell to enable complementary studies by DTA.

## III. EXPERIMENTAL RESULTS

### A. Results of *in situ* XRD experiments

The results from our *in situ* XRD experiments are summarized in Table I and Fig. 2. Experiment 1 was performed at ambient temperature only, with pressures up to 20.6 GPa. In good agreement with the previous studies,<sup>5,23,24</sup> two phase transitions were observed. The first transition from the ambient pressure phase II to phase III was completed at 1.4 GPa, while the second phase transition (III–VI) started at 18 GPa and was not completely finished until at the highest pressure of 20.6 GPa.

Experiments 2 and 3 were aimed at solving the structure in the  $P$ - $T$  region V, observed in the early experiments by Pistorius.<sup>23</sup> Both experiments showed that the phase in region V is identical to cubic phase VI. This is not completely unexpected if one considers the fact that a complete transition from phase III into the phase VI was still not achieved at 18 GPa at room temperature, but was easily accomplished by rapidly heating the pressure cell to 500 K at 10 GPa.<sup>5</sup> Figure 3 shows XRD patterns recorded in experiment 3, which

TABLE I. Experimental conditions for different runs.

Expt. No.	$\lambda$ (Å)	$P$ - $T$ path	Phase boundary crossed
1	0.711360	0–20.6 GPa, $T$ ambient	II/III, III/VI
2	0.711360	(a) Heating at 7.8–9 GPa up to 509 K (b) Decompression at 509 K from 7.5 to 4.2 GPa (c) Cooling at 4.2–5.6 GPa	III/V (8.7 GPa, ~430 K) V/III (~440 K)
3	0.711360	(a) Heating at 5.1–5.4 GPa (b) Decompression at 503 K from 4.1 to 3.4 GPa (c) Cooling at 3.5–3.9 GPa	III/V (5.2 GPa, ~473 K) V/III (3.6 GPa, ~473 K)
4	0.711360	(a) Heating at 3–0.8 GPa up to 402 K (b) Cooling at 0.8 GPa to RT	III/I (0.8 GPa, 350 K) I/II (0.8 GPa, ~363 K)
5	0.41125	(a) Heating diagonal from 11.4 GPa and 293 K to 1.9 GPa and 490 K (b) Compression to 2.7 GPa (c) Cooling from 2.4 GPa and 460 K to 1.7 GPa and 362 K	III/I (3.2 GPa, 457 K) I/II (2.1 GPa, 409 K)

prove that at 5.2 GPa, the phase transition III–VI(V) occurs in the temperature range 459–481 K. Experiment 2 showed the same phase transition at higher pressures (~8.7 GPa) and lower temperature (~430 K). Therefore,  $P$ - $T$  regions V and VI correspond to the stability region of the same cubic phase that we denote hereafter as V.

Experiments 4 and 5 were aiming to characterize  $P$ - $T$  region IV, observed by Pistorius.<sup>23</sup> This narrow region is located in the  $P$ - $T$  diagram between the stability regions of phases III ( $Ama2$ ) and I ( $P6_3mc$ ). Therefore, both experiments were performed with very small temperature steps in order to enable detection of an anticipated intermediate phase. In both experiments, 4 and 5, region IV was scanned upon heating and cooling. Both experiments showed the same result: in a narrow  $P$ - $T$  interval, the  $Ama2$  and  $P6_3mc$  phases coexist (see Figs. 2 and 4), and no additional peaks that could be assigned to a new phase (presumably phase IV)

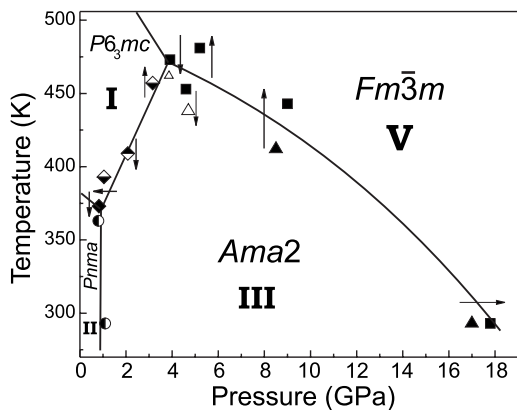


FIG. 2.  $P$ - $T$  diagram of  $\text{LiBH}_4$  based on data from the experiments summarized in Table I.

could be found. It should also be noted that regular (uniform) diffraction rings were recorded for the  $Ama2$  phase, while after the transition into the hexagonal  $P6_3mc$  phase, the rings consisted of sharp spots coming from a grainy single-crystal-like sample. The final cooling run in experiment 4 was performed at lower pressure (0.8 GPa) and showed a phase transition below 373 K from phase I ( $P6_3mc$ ) into ambient pressure phase II ( $Pnma$ ).

It seems unlikely that a hypothetical phase IV was missed in our experiments, both because of the small scan steps used and because of the observed coexistence of phases I ( $P6_3mc$ ) and III ( $Ama2$ ). Thus, our XRD study indicates that narrow  $P$ - $T$  region IV, identified from the volumetric and DTA experiments,<sup>23</sup> does not correspond to an anticipated intermediate phase IV.

From the results presented in this section, we were able to observe phase boundaries for all known phases of  $\text{LiBH}_4$  and to identify  $P$ - $T$  regions IV and V. Region V corresponds to cubic phase VI, recently found at 8–18 GPa and room

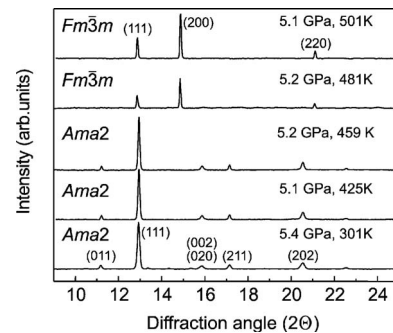


FIG. 3. XRD patterns recorded during heating in experiment 3. The phase transition from phase III ( $Ama2$ ) into phase VI ( $Fm\bar{3}m$ ) is clearly visible.

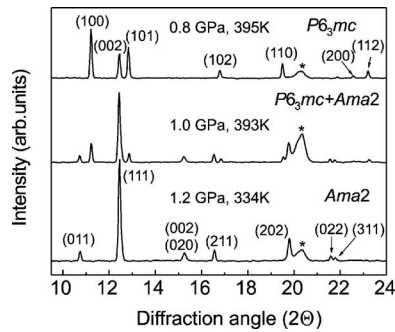


FIG. 4. XRD patterns recorded in experiment 4 close to the boundary between phase III (*Ama2*) and phase I ( $P6_3mc$ ) in conditions of quasi-isobaric heating. The pattern shown in the middle shows peaks from both phases. No additional peaks due to phase IV could be found. Asterisks mark the gasket peaks.

temperature.<sup>5</sup> Region IV does not correspond to any new individual crystallographic phase. In order to verify these results and reveal the nature of narrow region IV, we used thermal conductivity measurements as a complementary probe to study the I–III transition.

### B. Thermal studies of phase boundaries

To verify the existence and positions of the phase boundaries observed in the low-pressure range by Pistorius,<sup>23</sup> we also carried out DTA and thermal conductivity measurements, i.e., partly with the same technique as employed in Ref. 23. In particular, since we were not able to confirm the existence of phase IV by XRD, we used the quasicontinuous data to find evidence for hypothetical phase IV. As in earlier studies,<sup>13,24</sup> the thermal conductivity data showed large, repeatable anomalies at the phase boundaries. We show in Figs. 5 and 6 the data obtained on crossing the I–(IV)–III phase boundary twice at 1.2 GPa, first on cooling and then on heating. Data from DTA measurements [Fig. 5(a)] for the specific heat [Fig. 5(b)] and for the thermal conductivity [Fig. 5(c)] all show anomalies of the type expected at the

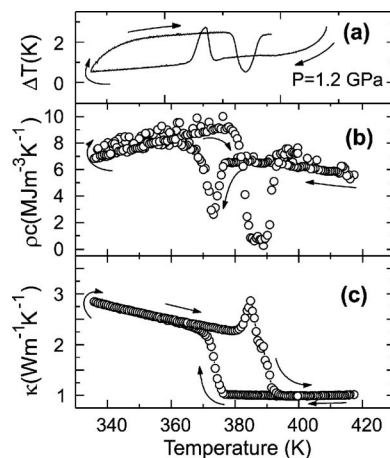


FIG. 5. Thermal data obtained during a first heating run at 1.2 GPa. (a) DTA data, (b) specific heat, and (c) thermal conductivity.

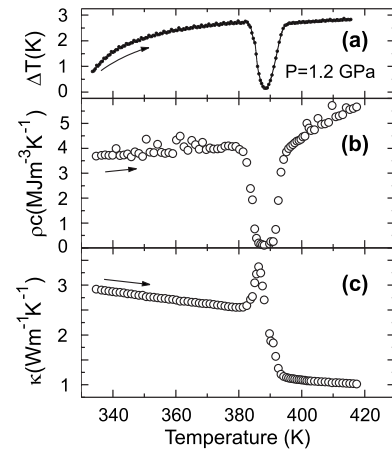


FIG. 6. Thermal data obtained during a subsequent cooling/heating cycle at 1.2 GPa immediately following the heating in Fig. 5: (a) DTA data, (b) specific heat, and (c) thermal conductivity.

structural phase transition. The thermal conductivity changes by more than a factor of 2 on going from well ordered phase III to orientationally disordered (see below) phase I. The temperature dependence for phase III is also compatible with the expected  $1/T$  dependence for ordered crystals, while for phase I, the thermal conductivity is weakly dependent on temperature. Except for the transition peaks, which are dynamic effects inherent to the method used, the isochoric specific heat changes only slightly. Close scrutiny reveals slight anomalies in the transition peaks on heating (see Figs. 5 and 6), with a tendency toward a double peak structure in the transition anomalies for both the specific heat and the thermal conductivity, as well as in the DTA data. The two sub-peaks are 4–5 K apart, in reasonable agreement with the width of region IV observed by Pistorius.<sup>23</sup>

On cooling, on the other hand, only DTA shows a similar behavior of a somewhat anisotropic peak. Comparing the data for heating and cooling, we find a hysteresis span of about 10 K, typical for a first-order transformation. The thermal data thus neither clearly confirm nor rule out the existence of the intermediate phase. However, our analysis of the phase transition mechanisms given in Sec. IV C below may provide an explanation of the origin of the observed anomaly even in the absence of the latter.

Our thermal conductivity and DTA measurements verified the existence and location of the I–II  $LiBH_4$  phase boundary given by Pistorius,<sup>23</sup> and complemented our earlier studies<sup>24</sup> of the strongly hysteretic low-temperature II–III phase boundary of  $LiBH_4$  by measurements up to 340 K. Above  $\sim 300$  K, the hysteresis width of the II–III boundary is almost temperature independent. The III  $\rightarrow$  II transition line accurately extrapolates the trend found earlier,<sup>24</sup> while the corresponding line for the II  $\rightarrow$  III transition runs parallel to it at a pressure about 0.25 GPa higher (or 60 K lower), such that the average transition pressure extrapolates accurately to the triple point suggested by Pistorius, which is near 0.9 GPa and 360 K.<sup>23</sup> However, as shown earlier,<sup>24</sup> the II  $\rightarrow$  III transition line turns sharply away from the temperature axis below 300 K, indicating a very high-energy threshold for the formation of phase III. At low temperatures, formation of

this phase is energetically unfavorable at low pressures presumably due to a high energetic barrier, and the structural transformation occurs only at pressures near 0.7 GPa. Once formed, on the other hand, phase III is stable down to zero pressure at all temperatures below 200 K.

#### IV. PHASE TRANSITION MECHANISMS AND ORDER PARAMETERS

A brief review of the phase symmetries and phase boundaries displayed on the  $P$ - $T$  diagram of  $\text{LiBH}_4$  raises questions which can be understood only in the framework of a unifying model of phase transitions. Indeed, four among the five observed transformations (I-II, II-III, I-III, and I-V) break the “group-subgroup” relationship between space groups. They have to be considered as reconstructive, requiring, therefore, a special approach.<sup>28</sup> The transformation from orthorhombic centrosymmetric structure II to orthorhombic polar structure III could be considered as an ordinary ferroelectric transition  $mmm$ - $mm2$ , however, the translational symmetry increases (the number of the f.u. in the cell decreases) at the transformation II-III, which is in contrast to the conventional ferroelectric transition where the paraelectric structure has a translational symmetry higher than a polar one. In order to work out a unifying model for pressure/temperature induced transformations observed in  $\text{LiBH}_4$ , we consider, in this section, structural mechanisms for the transitions.

For this purpose, the  $P$ - $T$  phase diagram of  $\text{LiBH}_4$  can be conditionally divided into two domains: (i) a “hexagonal” one, which includes the stability domains of phases I and II and (ii) a “cubic” one, covering the stability domains for phases III and V (Fig. 2). The attribution will be evident later on, after analysis of the corresponding structures and transformation mechanisms.

##### A. Hexagonal branch and its order parameters

A simple look at the structures of phases I and II, stable at ambient pressure, reveals a common hexagonal motive [Figs. 7(b) and 7(c)]. One easily finds a virtual superstructure, common for the structures of both hexagonal phase I and orthorhombic phase II, which can be reached by small restoring deformations of the latter two. This allows us to identify the mechanism that transforms the hexagonal parent (but latent) phase [Fig. 7(a)] into the two lower-symmetry phases, I and II. The symmetry of the hypothetical parent phase is  $P6_3/mmc$  (number of  $\text{LiBH}_4$  units per the unit cell  $Z=2$ ), and the Li and B atoms occupy Wyckoff positions  $2(c)$  and  $2(d)$ , respectively. Eight hydrogen atoms are randomly distributed among the positions  $4(f)$  and  $24(l)$ , resulting in an orientational disorder of the borohydrate tetrahedra [Fig. 8(a)]. A straightforward group-theoretical analysis (see, for example, Ref. 29) identifies two order parameters: (i) the one-component  $A_{2u} \equiv \Gamma_2^-$  at the Brillouin zone (BZ) center, associated with the transformation  $P6_3/mmc(Z=2) \rightarrow P6_3mc(Z=2)$ ; and (ii) the three-component  $M_2^-$  at the BZ boundary point  $M$  ( $\mathbf{q}=\mathbf{b}_1/2$ ), with only one of the components becoming nonzero at the transition  $P6_3/mmc(Z=2) \rightarrow Pnma(Z=4)$ .

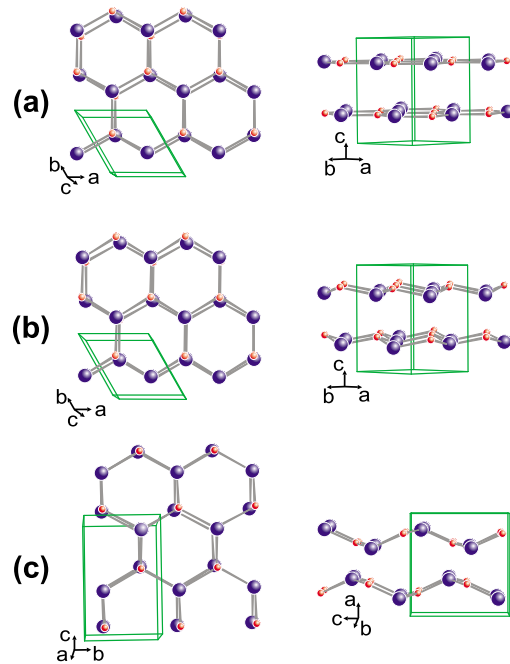


FIG. 7. (Color online) Lithium-boron framework of  $\text{LiBH}_4$  in (a) the latent phase  $P6_3/mmc$ , (b) high-temperature phase  $P6_3mc$ , and (c) orthorhombic  $Pnma$

The combined ordering and displacive mechanism for the transition from the parent  $P6_3/mmc(Z=2)$  phase to the  $P6_3mc(Z=2)$  phase consists of (i) a one-dimensional orientational ordering of the  $\text{BH}_4$  tetrahedra [Fig. 8(b)] and (ii)

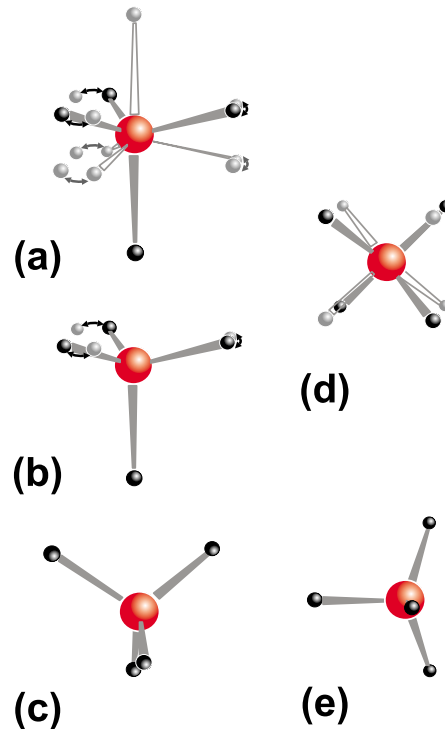


FIG. 8. (Color online) Orientation of tetrahedral  $\text{BH}_4$  anions in structures of (a) the latent hexagonal  $P6_3/mmc$ , (b)  $P6_3mc$ , (c)  $Pnma$ , (d)  $Fm\bar{3}m$ , and (e)  $Ama2$  phases.

antiparallel shifts of cation and anion flat layers along the sixfold axis of the structure, without distorting the in-layer hexagonal motive [Fig. 7(b)].

A similar combined mechanism corresponds to the second order parameter. It brings  $\text{LiBH}_4$  from the parent phase to phase II. As in the previous case, there is a combination of two mechanisms. The  $\text{BH}_4$  tetrahedra become ordered in the orthorhombic structure, while critical atomic displacements distort cation and anion layers [Fig. 7(c)]. Here, not only antiparallel shifts of the layers as a whole take place, but slight antiparallel displacements of ions perpendicular to their average planes also occur. One finds an epitaxial relationship between the hexagonal and orthorhombic lattices,

$$\mathbf{a}_0 = \mathbf{c}_h, \quad \mathbf{b}_0 = -(\mathbf{a}_h + \mathbf{b}_h), \quad \mathbf{c}_0 = \mathbf{a}_h - \mathbf{b}_h. \quad (1)$$

The correlation link, via BZ interior, between the irreducible representations of the two order parameters,  $\Gamma_2^- - \Sigma_1 - M_2^-$ , corresponds to two longitudinal branches in the phonon spectra of  $\text{LiBH}_4$ . An eigenvector of the corresponding phonons has the symmetry of the critical atomic displacements that create new phases. Those phonons we call “critical phonons,” having in mind only the symmetry aspect but not its soft mode behavior. One of those phonon branches, the low-energy acoustic one, involves parallel displacements of anion and cation layers along the sixfold axis. The other, a higher-energy optical one, shifts the anion and cation layers in opposite directions. Due to its identical symmetry, both distortions contribute to the symmetry-breaking mechanism, even if in a phenomenological theory a single critical set of irreducible representations will appear.

We end this part of the analysis by the following comments. (i) Both identified mechanisms are of “Landau type,” i.e., the corresponding transformation paths go from a high-symmetry phase to a low-symmetry one, satisfying the group-subgroup relationship. Thus, the observed I-II phase transformation is a transition between two low-symmetry structures (subgroups) of a single parent phase (supergroup). (ii) All described mechanisms are “primary” (symmetry breaking). (iii) The transformation I-II corresponds to switching between two order parameters,  $\Gamma_2^-$  and  $M_2^-$ , and each of the observed structures relates to a single order parameter. (iv) Nonsymmetry-breaking macroscopic distortions are rather small in the low-symmetry structures. For example, the components of the strain tensor, induced by the  $P6_3mc(Z=2) - Pnma(Z=4)$  transformation, are  $e_{11}=e_{22}=0.0250$ ,  $e_{33}=0.0148$ , and  $e_{12}=-0.0593$ .

### B. Transformation mechanism and order parameters for the cubic branch

The natural parent phase for observed high-pressure phase III is cubic  $\text{LiBH}_4$ -V, which has  $Fm-3m$  space group symmetry and 1 f.u. in the *primitive* unit cell ( $Z=1$ ).<sup>30</sup> Lithium and boron atoms occupy positions 4(a) and 4(b), respectively (Fig. 9), while hydrogen atoms randomly fill position 32(f) [Fig. 8(d)]. The mechanism of the V-III transformation combines, as for the hexagonal branch, ordering and displacive characters: (a) it stops the reorientational movement of the  $\text{BH}_4$  tetrahedra [Fig. 8(e)] and (b) two different displa-

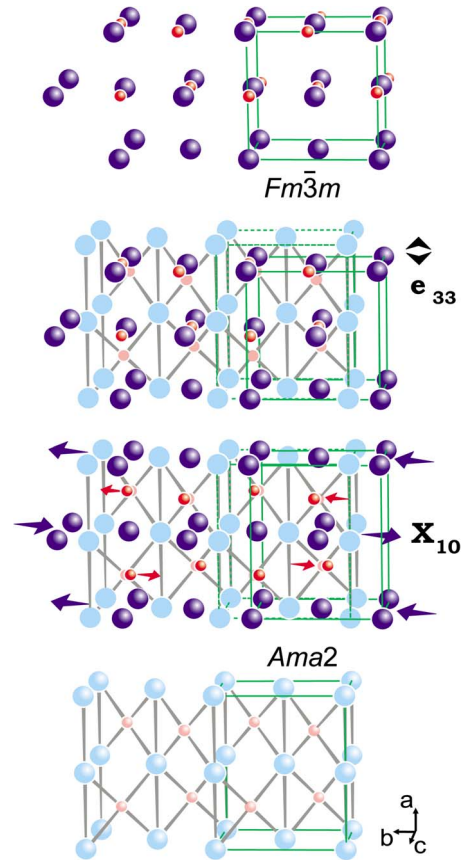


FIG. 9. (Color online) Mechanism of the  $Fm-3m$ - $Ama2$  transformation in  $\text{LiBH}_4$  (only lithium-boron sublattices are shown).

cive distortions establish the atomic arrangement characteristic of orthorhombic phase III. Again, the group-theoretical analysis identifies two corresponding order parameters: (i) the three-component  $F_{1u} \equiv \Gamma_4^-$  in the cubic BZ center and (ii) the six-component  $X_5^-$  at the BZ boundary point  $X$  [ $\mathbf{q}=(\mathbf{b}_1 + \mathbf{b}_2)/2$ ].<sup>29</sup> The former brings the cubic structure into a polar phase  $I4mm(Z=1)$ ; the latter induces a transition from the cubic parent phase to an orthorhombic  $Cmcm(Z=2)$ . A single component of either of the order parameters becomes nonzero at each transformation. However, both these low-symmetry phases are hypothetical, as they have never been observed in any experiment. A combined mechanism,  $\Gamma_4^- + X_5^-$ , transforms  $Fm-3m(Z=1)$  to  $Ama2(Z=2)$ , i.e., phase V to phase III.

Like in the hexagonal structure, two phonon branches with identical symmetry contribute to the mechanism distorting the cubic structure. First, a longitudinal acoustic phonon shifts cation and anion layers in the same direction. Second, a longitudinal optical mode drives their antiparallel displacements. The combined distortion mechanism for the  $Fm-3m(Z=1)$  to  $Ama2(Z=2)$  transformation is shown in Fig. 9. In addition to the primary order parameters just discussed, an important secondary mechanism should be mentioned. A uniaxial macroscopic deformation of the cubic crystal lattice,  $e_{33}$ , with the value of 0.265 is induced in the orthorhombic structure. It is an order of magnitude larger than the two other diagonal components of the spontaneous strain tensors,  $e_{11}=0.0358$  and  $e_{22}=0.0387$ . This reminds us of the case of

some reconstructive and martensitic transformations where spontaneous strains play an important role in the corresponding mechanisms,<sup>28</sup> although they are not primary order parameters. It is worth emphasizing that in contrast to the hexagonal branch, in the cubic domain, we observe a transition from the parent phase to the one distorted by the two order parameters simultaneously; neither of the two phases corresponding to an individual distortion has any stability region.

### C. Hexagonal-cubic transformations

Both parent structures, the hexagonal  $P6_3/mmc$  and the cubic  $Fm-3m$ , demonstrate direct relations to the close-packed structures, and therefore transitions between them and their derivatives can be considered in the framework of the corresponding crystallographic and group-theoretical schemes. A particular feature, important for understanding the mechanisms transforming hexagonal LiBH<sub>4</sub>-I and pseudohexagonal II to cubic V and pseudocubic III, is the “layer” character of the structures, i.e., identification of LiBH<sub>4</sub> layers as important building blocks. One can see (Fig. 7) that the hexagonal and pseudohexagonal structures of LiBH<sub>4</sub> show  $AB$  stacking of double (cation-anion) layers, while phases V and III (Fig. 9) form an  $ABC$  stacking sequence of similar double-layered packages. Thus, the evident mechanism for moving from the hexagonal domain of the phase diagram to the cubic one is, by analogy with the transition between close-packed structures,<sup>31</sup> a reshuffling of the cation-anion double layers, which occurs along with simultaneously induced in-layer distortions. Considering such a mechanism, we can express the basic vectors of the hexagonal unit cell as functions of the basic vectors of the primitive part of the face-centered cubic unit cell,

$$\mathbf{a}_h = -\mathbf{a}_C - \mathbf{b}_C, \quad \mathbf{b}_h = \mathbf{a}_C - \mathbf{c}_C, \quad \mathbf{c}_h = 2(\mathbf{a}_C + \mathbf{b}_C + \mathbf{c}_C)/3. \quad (2)$$

Then, from Eq. (2), one gets the maximal hexagonal subunit common to the cubic and hexagonal cells,

$$\mathbf{a}_h = 2\mathbf{a}_L + \mathbf{b}_L, \quad \mathbf{b}_h = \mathbf{a}_L + 2\mathbf{b}_L, \quad \mathbf{c}_h = 2\mathbf{c}_L,$$

$$\mathbf{a}_C = \mathbf{a}_L + \mathbf{b}_L + \mathbf{c}_L, \quad \mathbf{b}_C = -\mathbf{a}_L + \mathbf{c}_L; \quad \mathbf{c}_C = -\mathbf{b}_L + \mathbf{c}_L. \quad (3)$$

The latent high-symmetry structure belongs to the space group  $P6/mmm$ , in which cations and anions fill, with equal probability, position 1( $a$ ). It presents, therefore, a disordered polytype consisting of a random stacking of hexagonal cation-anion packages.

The reshuffling mechanism is known to create a significant energy barrier, which very well correlates with our observation of a high formation barrier for phase III (see Sec. III B). It has also been shown<sup>31</sup> that the thermodynamic character of such a reconstructive transformation, first order by definition, can vary from slightly to strongly discontinuous. These facts may be directly related to the complex character of the transition process between phases I and III. In contrast to the other transitions in the LiBH<sub>4</sub>  $P$ - $T$  diagram, this transition combines mechanisms evolving with different time scales, i.e., with different kinetics. Reshuffling is character-

ized by hindered kinetics, due to the corresponding high-energy barriers, while low-energy orientational ordering of tetrahedral anions is fast. The diffuse steplike anomalies in the thermal properties, observed at the transition from phase I to III, both in this work and in Ref. 23, can result, therefore, from the two-stage transformation process.

### D. Order parameters and local phase diagrams

The group-theoretical analysis presented in Secs. IV A and IV B allowed us to identify four order parameters for the phase transitions in the  $P$ - $T$  phase diagram of LiBH<sub>4</sub>. It would be a challenging exercise to investigate the corresponding theoretical models with the aim to work out its general phase diagram. However, even considering local models for the hexagonal and cubic domains, we arrive below to some important general conclusions. Another simplification consists in considering, without losing significantly in generality, one-dimensional effective order parameters instead of the multicomponent ones. This is well justified by the fact that only a single component of either multicomponent order parameter becomes nonzero at any phase transition observed in LiBH<sub>4</sub>.

The transformation properties of order parameter components described by the matrices of the corresponding irreducible representations define the same effective Landau free energy for both hexagonal and cubic order parameters:

$$F(\eta, \xi) = a_1 \eta^2 + a_2 \eta^4 + a_3 \eta^6 + b_1 \xi^2 + b_2 \xi^4 + b_3 \xi^6 + \gamma \eta^2 \xi^2, \quad (4)$$

in which the lowest degree biquadratic coupling between single-component effective order parameters  $\eta$  and  $\xi$  has been included. The model with the potential described by Eq. (4) has already been comprehensively studied by Gufan and Larin<sup>32</sup> (see also Ref. 28). The coefficients  $a_3$  and  $b_3$  are assumed to satisfy the conditions  $a_3 > 0$  and  $b_3 > 0$ , ensuring the positive definiteness of  $F(\eta, \xi)$  even for large values of  $\eta$  and  $\xi$ . It is worth noting that the thermodynamic model of Eq. (4) is “structurally stable,” which means that it is complete, and the principal predictions concerning the singularity types are valid, even if, for example, the maximum degree of the free-energy expansion is increased.

The potential according to Eq. (4) yields the following equilibrium values for the phases:

$$\text{Phase 0: } \eta_0 = 0, \quad \xi_0 = 0 \quad (\text{parent } P6_3/mmc \text{ or } Fm-3m),$$

$$\text{Phase A: } \eta_A^2 = \frac{-a_2 \pm \sqrt{a_2^2 - 3a_1 a_3}}{3a_2}, \quad \xi_A = 0 \\ (P6_3mc/I4mm),$$

$$\text{Phase B: } \eta_B = 0, \quad \xi_B^2 = \frac{-b_2 \pm \sqrt{b_2^2 - 3b_1 b_3}}{3b_2} \\ (Pnma/Cmcm),$$

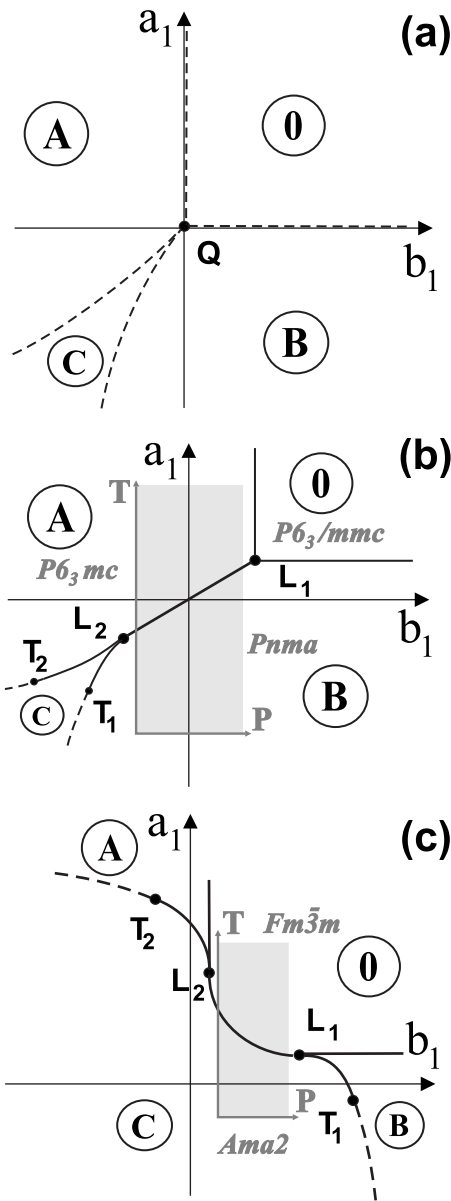


FIG. 10. Equilibrium phase diagram associated with the order-parameter expansion defined by Eq. (4) for (a)  $a_2 > 0$ ,  $b_2 > 0$ ,  $\gamma > 0$ ,  $\Delta > 0$ ; (b)  $a_2 < 0$ ,  $b_2 < 0$ ,  $\gamma > 2\sqrt{a_2 b_2} > 0$ ,  $\Delta > 0$ ; and (c)  $a_2 < 0$ ,  $b_2 < 0$ ,  $\gamma < -2\sqrt{a_2 b_2} < 0$ ,  $\Delta > 0$ . (b) Hexagonal and (c) cubic domains schematically shown as shadowed regions.

$$\text{Phase C: } \begin{cases} a_1 + 2a_2\eta_C^2 + 3a_3\eta_C^4 + \gamma\xi_C^2 = 0 \\ b_1 + 2b_2\xi_C^2 + 3b_3\xi_C^4 + \gamma\eta_C^2 = 0 \end{cases} \quad (\text{Pmc2}_1/\text{Ama2}). \quad (5)$$

The topology of the corresponding phase diagrams, shown in Fig. 10, depends on the values of the phenomenological coefficients  $a_i$  and  $b_i$ , assuming either a positive or a negative interaction  $\gamma$  between the two order parameters, as well as on the value of the determinant  $\Delta = 4a_2 b_2 - \gamma^2$ . Comparing topologies of the experimentally mapped phase diagrams (Fig. 2) and the diagrams predicted in the framework of the model based on Eq. (4), one concludes that the topology of Fig.

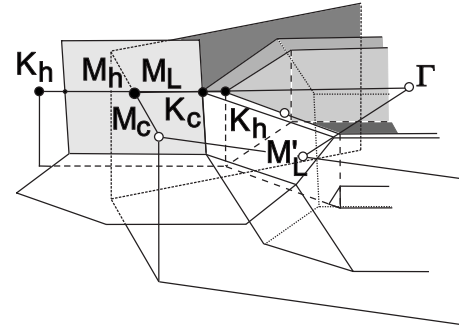


FIG. 11. Connection between the hexagonal ( $h$ ) and cubic ( $c$ ) Brillouin zones with the latent parent phase (L) BZ.

10(b) is relevant to the hexagonal domain of the  $P$ - $T$  diagram of  $\text{LiBH}_4$ , as it allows direct transition from phase I(A) to II(B). On the other hand, Fig. 10(c) corresponds to the cubic domain, where the first-order phase transition between V(0) and III(C) occurs.

Before moving to a discussion of the physical meaning of the phenomenological parameters, let us summarize the conclusions that can be drawn from a comparative analysis of the experimental and phenomenological phase diagrams, shown in Figs. 2 and 10. In order to minimize speculations, we restrict our analysis to details that are not affected by the model assumptions made above.

(i) The analysis clearly shows the important role of the *coupling between the order parameters* and its influence on the topology of the  $P$ - $T$  diagrams, the stability of the hexagonal and cubic structures (phases I and V), and their respective low-temperature derivatives (II and III). Indeed, a change in the sign of the coupling term  $\gamma$  induces a change in the layer stacking sequence length from two in the hexagonal branch to three in the cubic one. Although the line of transitions between the structures of the two branches is zigzag-like, it deviates only slightly from the vertical line on the  $P$ - $T$  diagram (Fig. 2), thus allowing us to conclude that pressure has a dominating role in reversing the sign of the coupling between the order parameters (phonon-phonon interaction).

(ii) Concerning the coefficients  $a_1$  and  $b_1$ , which are usually assumed to be linearly dependent on external variables,

$$a_1 = \alpha_0(T - T_C) + \alpha_1(P - P_C),$$

$$b_1 = \beta_0(T - T_C) + \beta_1(P - P_C), \quad (6)$$

one can see from a comparison of Figs. 2 and 11 that  $a_1$  corresponds mainly to the temperature variation ( $\alpha_0 \gg \alpha_1$ ), while  $b_1$  depends mainly on pressure ( $\beta_0 \ll \beta_1$ ).

## V. DISCUSSION

### A. Genesis of order parameters and origin of the structure instability

In Secs. IV A and IV B, we have identified the mechanisms destabilizing the crystal structure of  $\text{LiBH}_4$ . They are, in the hexagonal parent phase, zone-center phonon of symmetry  $\Gamma_2^-$  and zone-boundary phonon  $M_2^-$ . Both belong to the

same longitudinal acoustic and optical branches  $\Gamma_h-K_h-M_h$ . The cubic parent phase loses its stability with respect to a similar phonon pair; the  $\Gamma_4^-$  phonon at the  $\Gamma$  point and  $X_5^-$  on the BZ boundary, both belonging, again, to one acoustic and one optical branch in the direction  $\Gamma_C-K_C-X_C$ . We show now that the relevant acoustic and optical branches, in hexagonal and cubic structures, have the same distortive character, and they descend from the single acoustic-optic couple of branches in their common single-layered hexagonal superstructure characterized by the lattice vectors  $a_L$ ,  $b_L$ , and  $c_L$  in Eq. (3). Indeed, recalculating Eq. (3) for the reciprocal lattice vectors,  $\vec{b}_i^L$ , one finds the embedding geometry of three BZs corresponding to the hexagonal and cubic parent structures and their common hexagonal superstructure (for details, see Ref. 31). It is easy to see that the  $\Gamma_h-K_h-M_h$  segment, like the  $\Gamma_C-K_C-X_C$  one, correspond to the segment  $\Gamma_L-\Sigma_L-M_L$ . Indeed, the end points  $M_h$  and  $X_C$ , characterized by the vectors  $\vec{k}_{12}^h = \frac{1}{2}(\vec{b}_1^h + \vec{b}_2^h)$  and  $\vec{k}_{10}^c = \frac{1}{2}(\vec{b}_1^c - \vec{b}_3^c)$ , are given by the same vector  $\vec{k}_{12}^c = \frac{1}{2}\vec{b}_2^c$  in the latent phase BZ ( $M_L$  point; Fig. 11). The finishing geometrical stroke for proving the identity of the two order parameters in a latent single-layered hexagonal parent structure, identified by Eq. (3), is the longitudinal character of the two critical phonon branches. Thus, it turns out that, in spite of the different stacking sequences of the cation-anion double layers, the structures of the different  $\text{LiBH}_4$  phases show instability with respect to the same in-layer phonon modes. Our model assumption of the important role of the cation-anion packages in the structural design of  $\text{LiBH}_4$  therefore receives a strong support from thermodynamic and crystallographic considerations.

### B. Structural origin of the cation-anion layers

The existence of cation-anion layers in all four  $\text{LiBH}_4$  phases is suggested from the analysis of the atomistic mechanisms of phase transitions. This conclusion is not evident from a purely geometrical point of view. In order to justify this conclusion, let us consider crystal-chemical features of the structures of  $\text{LiBH}_4$  polymorphs.

Clear evidence for the existence of cation-anion layers is found in hexagonal phase I [Fig. 7(b)], where each  $\text{BH}_4$  tetrahedron has three short  $\text{B}\cdots\text{Li}$  contacts of 2.55 Å in the  $ab$  plane and one long  $\text{B}\cdots\text{Li}$  contact of 3.00 Å along the  $c$  axis. In orthorhombic phase II [Fig. 7(c)], these layers are corrugated and the structure is less anisotropic, with  $\text{B}\cdots\text{Li}$  distances of 2.37–2.55 Å within the layers and 2.57 Å between them. In the cubic branch, the existence of cation-anion layers is not so obvious. In phase III, the  $\text{BH}_4$  group is coordinated by four Li atoms at  $\text{B}\cdots\text{Li}$  distances of 2.35–2.66 Å in the square-planar configuration. The layers, where Li and  $\text{BH}_4$  groups are associated by means of the shorter  $\text{B}\cdots\text{Li}$  contacts, can be identified in the (011) plane in phase III (using the  $Ama2$  space group setting). The cubic structure of phase V is the most isotropic: each Li atom is octahedrally coordinated by six borohydride groups at identical  $\text{B}\cdots\text{Li}$  distances of 2.56 Å (18 GPa). Due to the high symmetry, different hypothetical layers can be identified here. However, only one type of layers is consistent both with geometrical considerations and with the phenomenological model. These

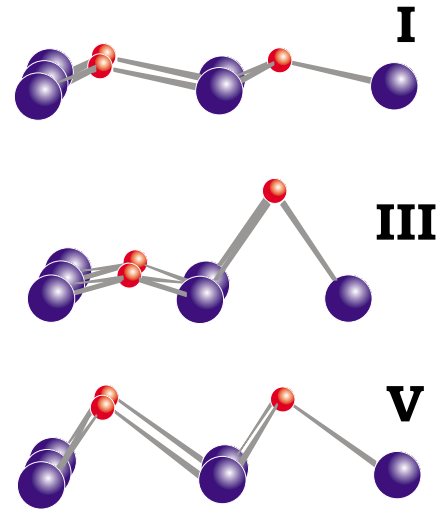


FIG. 12. (Color online) Cation-anion layers in the structure of different phases of  $\text{LiBH}_4$ . Only Li and B atoms are displayed. The character of the layer structure in phase III is seen to be intermediate between those of I and V.

cation-anion layers are situated in the (111) plane of the cubic structure, being very similar to those in phase I [Fig. 7(b)] and related to those in phase III by the mechanism described in Sec. IV B and shown on Fig. 9.

Clearly, the formation of layers in the  $\text{LiBH}_4$  structures is not determined by coordination polyhedra for the Li and  $\text{BH}_4$  groups, since the corresponding coordination numbers and geometries vary with pressure and temperature. Thus, the tetrahedral coordination of the  $\text{BH}_4$  anion by Li atoms dominates in phase II at ambient conditions, but at high temperature (phase I), it is deformed toward the trigonal coordination. At higher pressures (phase III), the  $\text{BH}_4$  anion shows the square-planar coordination, and at even higher pressures (phase V), the octahedral one. However, the variation of the coordination modes for the  $\text{BH}_4$  anion across the different structures is much more limited. In all four phases, the tetrahedral borohydride groups are connected to Li atoms via the tetrahedral edges, i.e., forming  $\text{BH}_2\cdots\text{Li}$  double bridges. The only exceptions are the  $\text{B}\cdots\text{Li}$  contacts in phase I and the shortest  $\text{B}\cdots\text{Li}$  contact in phase II (2.37 Å at 225 K), where the borohydride groups are connected to the respective Li atoms via the tetrahedral faces, i.e., forming  $\text{BH}_3\cdots\text{Li}$  triple bridges. Coordination via vertices, i.e., formation of  $\text{B-H}\cdots\text{Li}$  bridges, is absent in all four structures. The directional coordination of the  $\text{BH}_4$  group by Li atoms clearly indicates geometrical and possibly also electronic preferences of the  $\text{BH}_4\cdots\text{metal}$  atom ( $\text{BH}_4\cdots M$ ) interaction. The interaction of nonspherical  $\text{BH}_4$  anions with spherical Li cations results in cation-anion layers (Fig. 12), which determine the mechanisms of transitions between polymorphic structures. The directional interaction of tetrahedral  $\text{BH}_4$  with spherical metal atoms explains the relative complexity of the  $\text{LiBH}_4$  structures and of its  $P$ - $T$  phase diagram in comparison with  $\text{NaCl}$ , where both cation and anion are spherical.

The coordination rigidity of the  $\text{BH}_4\cdots M$  interaction has also been noticed in other systems, namely, in the extremely complex  $\text{Mg}(\text{BH}_4)_2$  structure<sup>33</sup> containing ten independent

$\text{BH}_4$  groups, all of them coordinated to Mg atoms via  $\text{BH}_2 \cdots \text{Mg}$  double bridges. It was also shown<sup>34</sup> that the directional  $\text{BH}_4 \cdots \text{Li}$  interaction, along with  $\text{NH}_2 \cdots \text{Li}$ , is structure determining in the mixed lithium-borohydride-amide system, namely, in  $\text{Li}_4(\text{BH}_4)(\text{NH}_2)_3$ . The  $\text{BH}_2 \cdots M$  double bridges dominate also in this mixed-anion system, as well as in other chemically modified metal borohydrides, such as a sodium borohydride complex with water,  $\text{Na}(\text{BH}_4)(\text{H}_2\text{O})_2$ .<sup>9</sup> Thus, we can conclude that the directional  $\text{BH}_4 \cdots M$  interaction in metal borohydrides results in the formation of anion-centered complexes, determining the structures of individual phases and the mechanisms of their polymorphic transformations. This hypothesis seems to be general for  $\text{BH}_4$ -containing systems and thus can be extended to predict structures and find the origin of phase transitions in other similar systems.

### C. Destabilization of borohydrides upon phase transition

Another application of combined crystal-chemical and phenomenological analysis of polymorphic transitions would be to reveal destabilization of borohydrides via formation of short  $\text{H} \cdots \text{H}$  distance and deformation of tetrahedral  $\text{BH}_4$  anions, both seen as steps toward destabilization of metal borohydrides.<sup>35,36</sup> A sign of such destabilization was observed in phase III, where these interactions were detected from the experiment and DFT calculations.<sup>5</sup> A similar destabilization in  $\text{LiBH}_4$  or related systems may be achieved during reconstructive phase transitions or melting. Indeed, some hydrogen desorption from  $\text{LiBH}_4$  occurs upon II-I transition ( $\sim 0.1$  wt % hydrogen loss) and on melting ( $\sim 1$  wt % of hydrogen loss).<sup>1</sup> We suggest that other phase boundaries in the  $P$ - $T$  phase diagram of pure or chemically modified  $\text{LiBH}_4$  should be addressed with respect to possible hydrogen desorption. Chemical modification of  $\text{LiBH}_4$ , for example, by exchanging a fraction of the  $\text{BH}_4$  anions by halide anions,<sup>2</sup> could be used along with pressure and temperature to investigate hydrogen desorption properties of modified  $\text{LiBH}_4$  within the  $P$ - $T$  phase diagram reported here.

## VI. CONCLUSIONS

A combination of diffraction, calorimetric, and transport experiments has uncovered a complex sequence of phase transformation of  $\text{LiBH}_4$  as a function of temperature and pressure. The experimentally found changes of symmetry have been rationalized in the form of a  $P$ - $T$  phase diagram and parametrized in the frame of Landau theory using group-theoretical concepts. The corresponding structural deformations have been analyzed in terms of symmetry-breaking atomic positional shifts, in agreement with experimental crystal structures. There are few findings that should be specially noted with respect to hydrogen storage properties.

(1) Both group-theoretical and crystal-chemical considerations reveal nontrivial layered structures in  $\text{LiBH}_4$ . The layers and their deformations seem to define the structural stability of the observed phases. Phases with strongly deformed layers should accumulate more tension in the  $\text{BH}_4$  units, thus affecting the stability of the complex anion.

(2) All the transitions are of the first order, and therefore the energy barrier for hydrogen desorption can be locally lowered by heterophase fluctuations and by nucleation and growth processes in the vicinity of the phase boundaries.

(3) Orthorhombic phase III is a polar one. However, in contrast to the conventional ferroelectric transition, the translational symmetry increases upon the II-III transition; this may lead to a nontrivial structural response to the electric field. In case of a strong coupling, the electric field may serve as one more parameter controlling the stability of crystal structure of polar phases III and I.

## ACKNOWLEDGMENTS

We acknowledge SNBL for in-house beam time allocation. Part of the x-ray data were collected at ID09A (ESRF) with the assistance of M. Hanfland. B.S. and A.V.T. also acknowledge financial support from Magn. Bergvalls Stiftelse and Carl Tryggers Stiftelse.

\*dmitriev@esrf.fr

<sup>1</sup>P. Maunon, F. Buchter, O. Friedrichs, A. Remhof, M. Biemann, C. N. Zwicky, and A. Züttel, *J. Phys. Chem. B* **112**, 906 (2008).

<sup>2</sup>L. Mosegaard, B. Moeller, J.-E. Jorgensen, Y. Filinchuk, Y. Cerenius, J. Hanson, E. Dimasi, F. Besenbacher, and T. Jensen, *J. Phys. Chem. C* **112**, 1299 (2008).

<sup>3</sup>F. E. Pinkerton, G. Meisner, M. Meyer, M. Balogh, and M. Kundrat, *J. Phys. Chem. B* **109**, 6 (2005).

<sup>4</sup>J. Yang, A. Sudik, D. J. Siegel, D. Halliday, A. Drews, R. O. Carter, C. Wolverton, G. J. Lewis, J. W. A. Sachtler, J. J. Low, S. A. Faheem, D. A. Lesch, and V. Ozolins, *Angew. Chem., Int. Ed.* **47**, 882 (2008).

<sup>5</sup>Y. Filinchuk, D. Chernyshov, A. Nevidomskyy, and V. Dmitriev, *Angew. Chem., Int. Ed.* **47**, 529 (2008).

<sup>6</sup>S. C. Abrahams and J. Kalnajs, *J. Chem. Phys.* **22**, 434 (1954).

<sup>7</sup>R. L. Davis and C. H. L. Kennard, *J. Solid State Chem.* **59**, 393

(1985).

<sup>8</sup>P. Fischer and A. Züttel, *Mater. Sci. Forum* **443-4**, 287 (2004).

<sup>9</sup>Y. Filinchuk and H. Hagemann, *Eur. J. Inorg. Chem.* (to be published).

<sup>10</sup>B. Sundqvist and O. Andersson, *Phys. Rev. B* **73**, 092102 (2006).

<sup>11</sup>R. S. Kumar and A. L. Cornelius, *Appl. Phys. Lett.* **87**, 261916 (2005).

<sup>12</sup>C. M. Araújo, R. Ahuja, A. V. Talyzin, and B. Sundqvist, *Phys. Rev. B* **72**, 054125 (2005).

<sup>13</sup>Y. Filinchuk, A. V. Talyzin, D. Chernyshov, and V. Dmitriev, *Phys. Rev. B* **76**, 092104 (2007).

<sup>14</sup>J.-Ph. Soulié, G. Renaudin, R. Černý, and K. Yvon, *J. Alloys Compd.* **346**, 200 (2002).

<sup>15</sup>M. R. Hartman, J. J. Rush, T. J. Udovic, R. C. Bowman, Jr., and S. J. Hwang, *J. Solid State Chem.* **180**, 1298 (2007).

- <sup>16</sup>E. M. Fedneva, V. L. Alpatova, and V. I. Mikheeva, *Russ. J. Inorg. Chem.* **9**, 826 (1964).
- <sup>17</sup>S. Gomes, H. Hagemann, and K. Yvon, *J. Alloys Compd.* **346**, 206 (2002).
- <sup>18</sup>Y. Nakamori and S. Orimo, *J. Alloys Compd.* **370**, 271 (2004).
- <sup>19</sup>K. S. Gavrichev, *Inorg. Mater.* **39**, S89 (2003).
- <sup>20</sup>Y. Filinchuk and D. Chernyshov, *Acta Crystallogr., Sect. A: Found. Crystallogr.* **A63**, s240 (2007).
- <sup>21</sup>Z. Łodziana and T. Vegge, *Phys. Rev. Lett.* **93**, 145501 (2004).
- <sup>22</sup>N. A. Zarkevich and D. D. Johnson, *Phys. Rev. Lett.* **100**, 040602 (2008).
- <sup>23</sup>C. W. F. T. Pistorius, *Z. Phys. Chem., Neue Folge* **88**, 253 (1974).
- <sup>24</sup>A. V. Talyzin, O. Andersson, B. Sundqvist, A. Kurnosov, and L. Dubrovinsky, *J. Solid State Chem.* **180**, 510 (2007).
- <sup>25</sup>P. Vajeeston, P. Ravindran, A. Kjekshus, and H. Fjellvåg, *J. Alloys Compd.* **387**, 97 (2005).
- <sup>26</sup>T. J. Frankcombe, G.-J. Kroes, and A. Züttel, *Chem. Phys. Lett.* **405**, 73 (2005).
- <sup>27</sup>J. Rodrigues-Carvajal, *Physica B* **192**, 55 (1993).
- <sup>28</sup>P. Toledano and V. Dmitriev, *Reconstructive Phase Transitions in Crystals and Quasicrystals* (World Scientific, Singapore, 1996).
- <sup>29</sup>H. T. Stokes and D. M. Hatch, *Isotropy Subgroups of the 230 Crystallographic Space Groups* (World Scientific, Singapore, 1988).
- <sup>30</sup>In group-theoretical considerations, it is convenient to use a primitive unit cell instead of the Bravais one. The latter is four times larger in the case of face-centered *F* lattices and twice as large for a base-centered *A* lattice.
- <sup>31</sup>V. P. Dmitriev, S. B. Rochal, Y. M. Gufan, and P. Toledano, *Phys. Rev. Lett.* **62**, 2495 (1989).
- <sup>32</sup>Yu. M. Gufan and E. S. Larin, *Sov. Phys. Solid State* **22**, 270 (1979).
- <sup>33</sup>R. Cerný, Y. Filinchuk, H. Hagemann, and K. Yvon, *Angew. Chem., Int. Ed.* **46**, 5765 (2007).
- <sup>34</sup>Y. E. Filinchuk, K. Yvon, G. P. Meisner, F. E. Pinkerton, and M. P. Balogh, *Inorg. Chem.* **45**, 1433 (2006).
- <sup>35</sup>W. Grochala and P. P. Edwards, *Chem. Rev. (Washington, D.C.)* **104**, 1283 (2004).
- <sup>36</sup>A. J. Du, S. C. Smith, and G. Q. Lu, *Phys. Rev. B* **74**, 193405 (2006).